Influence of mitral valve elasticity on flow development in the left ventricle

Chiara Celotto, Luigino Zovatto, Dario Collia, Gianni Pedrizzetti *

Department of Engineering and Architecture, University of Trieste, Italy

ARTICLE INFO

Accepted 12 November 2018

Keywords:
Left ventricle
Mitral valve
Immersed boundary method
flow–tissue interaction

ABSTRACT

The Mitral valve of the human heart has a great relevance for numerous cardiac pathologies; however, the knowledge of relationships between valvular properties and cardiac function is still limited. On one side, this is partly due to the limited resolution of clinical imaging technologies that do not allow routinely visualization of the valve during its motion. On the other, its modeling presents serious challenges either due to the strong flow–tissue interaction or because the mechanical properties of its constitutive elements are complex and not measurable *in vivo*. This work introduces a parametric model of the Mitral valve where the interaction with the blood flow obeys global balances and the overall elastic properties are summarized into a single functional parameter. This is integrated into a numerical model of left ventricular fluid dynamics with the aim to study the effect of varying the valvular stiffness. Results show that the elasticity of the valve influences the amplitude of the mitral opening, while the timings of opening/closure are driven by the transmitral blood flow due to the ventricular dynamics. In addition, the increase of stiffness increases the transvalvular pressure gradients required to ensure the same flow. These results are discussed in relation to parameters for monitoring valvular stiffness that are accessible through clinical imaging.

1. Introduction

Understanding the dynamics of the Mitral valve (MV) represents an important problem of fluid–tissue interaction (FTI) for its close link to the development and the progression of several cardiac diseases. Most common valvular diseases are MV prolapse, which causes blood regurgitation in the atrium chamber, and MV stenosis, which causes the leaflets to become stiff, resulting in a narrowed valve opening and reduced blood flow from the atrium to the ventricle. Computational models of the MV dynamics within the left ventricle (LV) permit to better understand the interaction between the blood flow and the valvular elements. However, modeling the dynamics of a natural MV is an open challenge and a complete description of the mitral dynamics during its interaction with the incoming flow is still lacking. In fact, time/space resolution of the in-vivo heart scans is still insufficient to provide a valid recording of the valve geometry during its motion. Furthermore, the mechanical properties of the valvular tissue, neither homogeneous nor isotropic, are known only approximately and on average terms.

To overcome these problems, some authors dealing with cardiac fluid motion treated the presence of the MV without an explicit modeling but, for example, imposing kinematic boundary conditions at the inlet orifice, varying the inclinations of the transmitral velocity or changing the inlet profile [1,2]. Although those procedures may be able to reproduce the principal characteristics of the intraventricular blood flow, they cannot provide a description of the FTI phenomena associated with MV motion. The first attempts to simulate and analyze the dynamics of a natural MV was made using the Immersed Boundary Method (IBM), a finite difference method that couples an Eulerian description for the blood flow to a Lagrangian description for the immersed structure [3,4]. The most recent and advanced IBM models include hyperelastic constitutive material models, finite strain deformations and geometries derived from in vivo experimental data [5–9]. Most of these presented fully integrated MV–LV models, in which the geometry is derived from clinical images and takes into account left ventricle contraction, nonlinear soft tissue mechanics as well as the fluid–structure interaction between the MV, LV and the blood and probably represent the most accurate FTI solution available to date [10]. However, the uncertainty of patient-specific parameter identification, the uncertainties in MV geometry reconstruction from imaging data and the limited information available on properties of the different MV elements do not ensure a superior accuracy of a complete MV modeling with respect to carefully designed inlet boundary conditions for LV fluid dynamics.

Physically, the MV leaflets are almost passive structures that open with the flow with minimal resistance (mainly due to their

* Correspondence to: Department of Engineering and Architecture, University of Trieste, P. Europa 1. 34127, Trieste, Italy.
E-mail address: giannip@dia.units.it (G. Pedrizzetti).

elastic response to bending, which involves slight deformations), with a geometric configuration that cannot vary much for a given degree of opening.

Therefore in this work, and with the perspective of potential clinical applications, we follow an intermediate approach between the complete modeling of FTI, which would require information about tissue properties that are not available at an individual level, and the usage of valveless orifices with given boundary conditions, which do not include any FTI effect. In this approach, the valve geometry is assumed as known and its motion is modeled with just one degree of freedom, the valvular opening (φ), while its dynamic equations are derived from integral balances. This MV model is included in a numerical solution of fluid mechanics based on the Immersed Boundary Method, with the blood modeled as a Newtonian incompressible fluid. The LV is described as a set of prescribed moving boundaries obtained from Magnetic Resonance Imaging (MRI) and its imposed motion represents the inner kinematic forcing condition of the system. The geometry of the MV, following a previous work [11], is here described by a mathematical model and its one-degree-of-freedom motion description allows a substantial simplification of the structural part in the FTI problem.

Whereas a complete modeling of tissue mechanics is best suited to uncover general physical/physiological phenomena of FTI in MV dynamics, this kind of models is potentially more adequate for clinical applications. The valve geometry can be evaluated from imaging in a few instants (typically in the fully-open and fully-closed configurations, that last little longer) and then its time-varying geometry reconstructed for various degrees of opening. The global elastic parameters can thus be estimated to ensure the functional congruence with few observable information about valve motion without requiring explicit knowledge of inaccessible tissue properties.

The proposed simplified approach is used here to better understand the role of elasticity, or stiffness, in the dynamics of the valve, to understand how it influences either the timing or the amplitude of MV motion. The analysis will be performed in the case of both a healthy and a pathological ventricle and the results are discussed in relation of clinical observables.

2. Methods

2.1. Mathematical definition of the mitral valve geometry

The mitral valve presents two distinct asymmetric leaflets: a larger one on the anterior side of the heart and a smaller posterior one. The geometry of the valve is described here by an analytical model as a two-dimensional surface [11]:

$$\begin{aligned} X_v(\vartheta, s) &= R\cos\vartheta\,(1 - s\cos\varphi) - \varepsilon R s\cos\varphi\,, \\ Y_v(\vartheta, s) &= R s\sin\vartheta\,(1 - sk\cos\varphi)\,, \\ Z_v(\vartheta, s) &= -s^2\left(\frac{1+k}{2} + \varepsilon\cos\vartheta + \frac{1-k}{2}\cos 2\vartheta\right) R s\sin\varphi\,. \end{aligned} \tag{1}$$

In this representation, s represents the longitudinal parametric coordinate, from the annulus to the trailing edge, and ϑ is the circumferential parametric coordinate as sketched in Fig. 1. The parameters R, ε and k are three characteristic parameters of the valve, whose values are fixed to a realistic set. $R = 1.1$ cm is the radius of the mitral annulus, $\varepsilon = 0.3$ is a dimensionless parameter representative of the asymmetry of the valve leaflets and $k = 1/3$ is a dimensionless parameter giving the degree of the ellipticity of the mitral orifice. The opening angle of the valve, φ, is the parameter describing the movement of the valve in a one-degree-of-freedom formulation; it normally spans from 0 (closed) to $\pi/2$ (fully open) and, for each intermediate value, the geometrical configuration of the valve is given by Eq. (1).

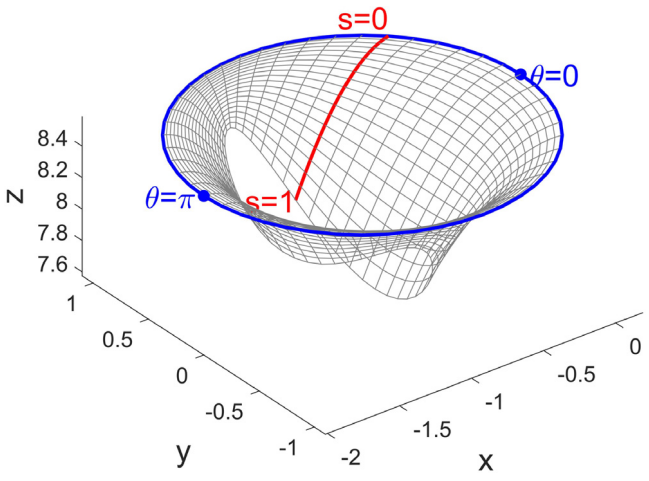

Fig. 1. Three-dimensional view of the valve with indication of the parametric coordinates. The longitudinal coordinate s spans from the annulus ($s = 0$) to the trailing edge ($s = 1$). The circumferential coordinate ϑ originates from the anterior side in the anti-clockwise direction (seen from top). The anterior leaflet is centered at $\vartheta = 0$ while the posterior leaflet is centered at $\vartheta = \pi$. Graph refers to $\varphi = \pi/4$.

The analytic geometry (1) was chosen for its simplicity and for reproducibility; however, any more realistic geometry $\boldsymbol{X}_v(\vartheta, s)$, either analytical [6,12] or extracted from images, could be used. The simple shape (1) has several limitations. The mitral annulus is modeled with a circular planar profile and constant dimension, whereas, from an anatomical point of view, it has a three-dimensional saddle shape that relaxes during diastole, slightly increasing its area compared to systole. Furthermore, the commissure of the Mitral valve, which is here modeled as a straight segment, is rather a more C-shaped line. From an anatomical point of view the leaflets are connected to the LV walls by chordae tendinae, tendons that originate from the papillary muscles at the base of the ventricle and have the function to prevent the eversion of the flaps in presence of high ventricular pressure during systole. Those tendons are not modeled in this work but their role is simulated imposing that the valve cannot move beyond the complete closure $\varphi = 0$.

2.2. Left ventricle geometry

The LV geometry is reconstructed from clinical MRI recordings as previously described [13], which provided the coordinates of some material points during the heartbeat. The LV surface is described by the position vector $\boldsymbol{X}(\vartheta, s)$ that depends on the parametric coordinate ϑ along the circumference and the longitudinal one s from the annulus to the LV apex, as sketched in Fig. 2.

The analysis is performed in correspondence to two different LV geometries, one from a healthy subject and one from a patient with a dilated cardiomyopathy. The tele-diastolic volume of the normal ventricle is 113.48 ml while that of the dilated ventricle is 199.30 ml. The ejection fractions of the normal ventricle and of the dilated ventricle are equal to 59% and to 29% respectively; Fig. 3 shows the geometry of the two LVs and the volumetric profiles.

A portion of the aortic artery and a portion of the atrium, modeled as tubular structures, are included for avoiding the formation of jets and mixing in the open space external to the ventricle (Fig. 4). Finally, the circular aortic valve (with radius 0.75 cm) is modeled simply as a plane wall which is either fully opened (systole) or fully closed (diastole).

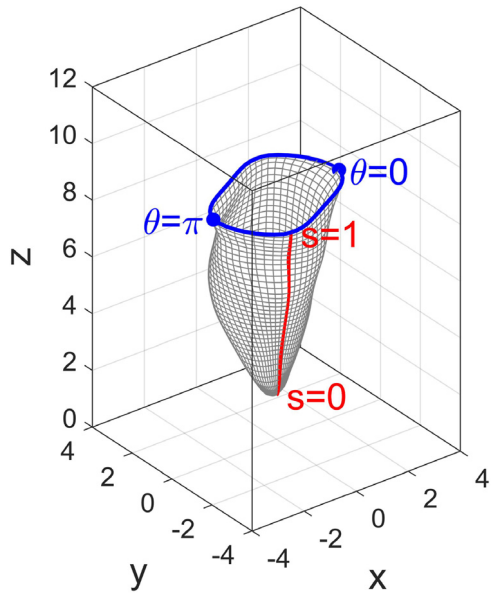

Fig. 2. Three-dimensional view of the healthy LV wall with indication of the parametric coordinates. The longitudinal coordinate s spans from the apex ($s = 0$) to the valvular plane ($s = 1$). The circumferential coordinate ϑ starts from 0 on the positive x axis in the anti-clockwise direction.

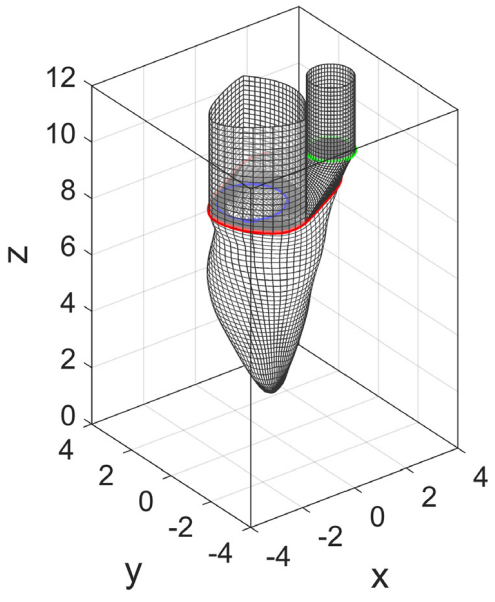

Fig. 4. Three-dimensional view of the complete geometrical model used in the simulation in the case of healthy ventricle.

2.3. Mathematical definition of the mitral valve motion

The motion of the valve leaflets is described by deriving a differential equation for the opening angle. Extending a previous formulation [11], the mitral valve motion is driven by the blood flow and it is hampered by the resistance to deformation due to its small stiffness.

The contribution due to the flow is determined, instant by instant, by imposing the conservation of mass at an integral level assuming a valve that would move without any resistance other than maintaining its own shape. For this purpose, we first consider the rate of volume of fluid crossing the valve

$$\mathrm{I_f}\,(\mathrm{t},\varphi) = \int_{S_{MV}} (\mathbf{v}\cdot\mathbf{n})\,\mathrm{d}S; \tag{2}$$

where $\mathbf{v}$ is the local fluid velocity, S_{MV} is the surface of the MV and $\mathbf{n}$ is the unitary normal to the surface. For mass conservation, the integral (2) should be equal to the rate of volume of fluid spanned by the moving valve

$$\mathrm{I}_v\,(\mathrm{t},\varphi) = \int_{S_{MV}} (\boldsymbol{V}_\mathrm{v}\cdot\mathbf{n})\,\mathrm{d}S; \tag{3}$$

where $\boldsymbol{V}_v$ is the velocity of the valve material points. Recalling that the valve geometry $\boldsymbol{X}_v\,(\vartheta,\mathrm{s})$ is described in function of the valvular opening then the velocity can be expressed in general as

$$\boldsymbol{V}_v\,(\vartheta,\mathrm{s}) = \frac{d\boldsymbol{X}_v}{d\varphi}\frac{d\varphi}{dt}; \tag{4}$$

proportional to $d\varphi/dt$. Therefore, the integral (3) can be rewritten as

$$\mathrm{I}_v\,(\mathrm{t},\varphi) = \mathrm{I}_0\,(\varphi)\,\frac{\mathrm{d}\varphi}{\mathrm{dt}}; \tag{5}$$

where I_0 is the integral (3) computed with velocity for unitary rate of opening, $\boldsymbol{V}_v = d\boldsymbol{X}_v/d\varphi$.

An application of mass balance in global terms results in the equality between the volume of fluid crossing the valve and that allowed by valvular displacement. Therefore, equating Eqs. (2) and (5), gives the differential equation that governs the motion of a

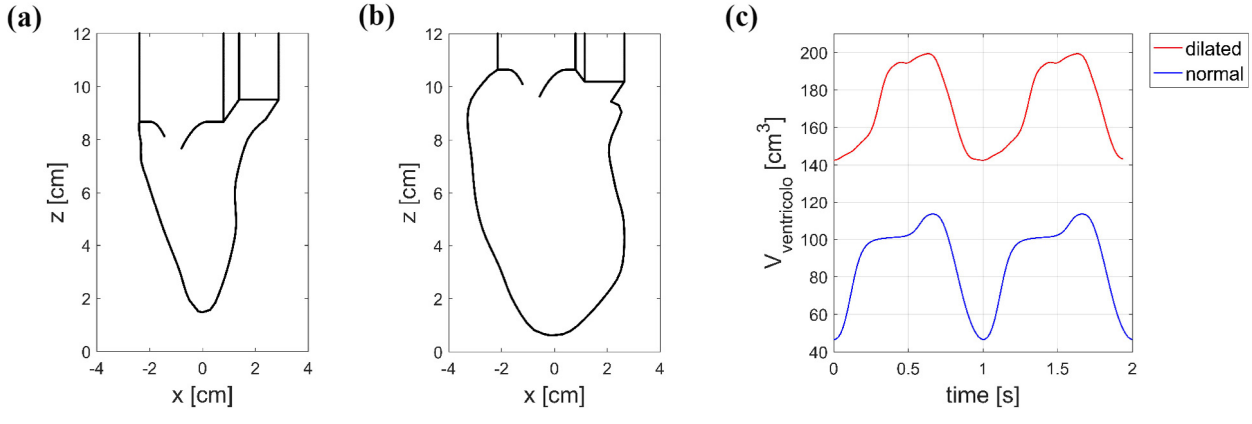

Fig. 3. Two-dimensional longitudinal section of a healthy ventricle (a) and a dilated ventricle (b) at the end of systole ($t = 0$) on a plane parallel to the z-axis passing containing both valves; and (c) corresponding time profiles of the LV volume.

valve completely driven by the blood flow, without any additional resistance

$$\frac{d\varphi}{dt} = \frac{I_f(t,\varphi)}{I_0(\varphi)} = I(t,\varphi)\,. \tag{6}$$

This equation represents the equation of motion for a valve with no elastic recall. Since the density of the valve is comparable to the one of the fluid it is immersed in, the valve is here considered massless, thus the absence of the acceleration term.

The elastic resistance due to the deformation of the valve induces a second term to be added in Eq. (6) that depends on the tissue elasticity and can be estimated from global considerations.

To describe the tissue behavior in global terms we have adopted a neo-Hookean, homogeneous isotropic and incompressible material model, therefore the elastic energy stored in the deformed body is given by the strain energy function (SEF)

$$SEF = C * W = C * (\mathcal{I} - 3)\,; \tag{7}$$

where $W = (\mathcal{I}-3)$ is the dimensionless strain energy function, and $\mathcal{I} = {\lambda_1}^2 + {\lambda_2}^2 + {\lambda_3}^2$ is the first invariant of the deformation tensor (where λ_i are the principal deformations). In this formulation, the value $J = 3$ represents the reference zero corresponding to the absence of deformation (all $\lambda_i = 1$). Finally, C represents a dimensional elasticity constant that globally characterizes all the unknown properties of the leaflets material. When dealing with continuous medium subjected to large deformations, the restoring force can be derived by the differential of the strain energy function with respect to the appropriate measures of deformations. In this case, any deformation depends on a single parameter, the opening angle φ, therefore, the elastic restoring force can be formally written

$$R(\varphi) = \frac{d(SEF)}{d\varphi} = C\left(\frac{dW(\varphi)}{d\varphi}\right) = CF(\varphi); \tag{8}$$

where C also depends on the adopted deformation tensor in the evaluation of the strain energy function.

The equation that governs the motion of the massless valve is thus obtained by combination of the forcing term (6) and the resistance term (8) which is added to include the elastic recall

$$\frac{d\varphi}{dt} = I(t,\varphi) - CF(\varphi)\,; \tag{9}$$

In this formulation all the material and geometrical properties of the valve are included in the coefficient C; which becomes, dimensionally, the inverse of a characteristic time of elastic closure.

The equation of motion (9) does not include the inertia of the valve that is assumed with no added mass with respect of the surrounding fluid; differently, the fluid inertia is implicitly accounted in the formulation (6) or (9). In fact, while in a complete fluid–structure interaction model the fluid inertia is included by fluid pressure, in this formulation the valve moves accordingly to the fluid velocity, and the dynamics of the fluid is dictated by the complete Navier–Stokes equations. Therefore, the velocity values of the fluid that surrounds the valve and that drives its motion evolve following dynamic equations that include the inertia of the fluid itself.

Eq. (9) requires to evaluate the function $W(\varphi)$ that is obtained from the first invariant of the deformation tensor $\mathcal{I}$. Since the valve is modeled as a two-dimensional spatial surface (1), the deformations can be described for each value of the opening angle φ by a symmetric 2×2 tensor, starting from the undeformed configuration at $\varphi = 0$. The generic strain tensor is evaluated through the integration over time of the strain rate tensors. The strain rate tensor $\mathbf{SR}(s,\vartheta,t)$ is the symmetrical part of a tensor $\boldsymbol{S}(\boldsymbol{\xi},t)$ which is the time derivative of the deformation gradient tensor $\boldsymbol{F}$

$$\mathbf{S}(\boldsymbol{\xi},t) = \frac{\partial \mathbf{F}}{\partial t} = \frac{\partial}{\partial t}\left[\frac{\partial \boldsymbol{X}_\mathbf{v}(\mathbf{X},t)}{\partial \boldsymbol{\xi}}\right] = \frac{\partial}{\partial \boldsymbol{\xi}}\left[\frac{\partial \boldsymbol{X}_\mathbf{v}(\mathbf{X},t)}{\partial t}\right]$$

$$= \frac{\partial}{\partial \boldsymbol{\xi}}\left[\mathbf{v}_\mathbf{v}(\mathbf{X},t)\right]; \tag{10}$$

where $\boldsymbol{\xi}$ stands formally for the physical spatial coordinates of the material points on the valvular surface. Thus the individual component of $\mathbf{SR}(s,\vartheta,t)$ can be expressed

$$SR_{ij} = \frac{1}{2}\left(S_{ij} + S_{ji}\right) = \frac{1}{2}\left(\frac{1}{h_j}\frac{\partial \boldsymbol{V}_\mathbf{v}}{\partial x_j}\boldsymbol{\tau}_i + \frac{1}{h_i}\frac{\partial \boldsymbol{V}_\mathbf{v}}{\partial x_i}\boldsymbol{\tau}_j\right); \tag{11}$$

where the indices i and j take the value s or ϑ. The $\boldsymbol{\tau}_i(s,\vartheta,t)$ are the local unit tangent vectors and $h_i(s,\vartheta,t)$ are the metric coefficients, the physical lengths of the unit coordinates increment [14].

The strain rate tensor $\mathbf{SR}(s,\vartheta,t)$ is proportional to the gradient valvular velocity, and the latter can be expressed as proportional to $\partial\varphi/\partial t$ with a proportionality constant that depends on the differential deformation associated to the different geometric configuration expressed by the angle φ. Therefore, in analogy to (5), the strain rate tensor can be expressed as

$$\boldsymbol{SR}(s,\vartheta,t) = \mathbf{SR}_0(s,\vartheta,\varphi)\frac{d\varphi}{dt}; \tag{12}$$

where $\mathbf{SR}_0$ is the unitary strain rate tensor, computed from (11) with unitary rate of opening, $\boldsymbol{V}_v = d\boldsymbol{X}_v/d\varphi$, that expresses the changes in valvular deformation when varying the parameter φ. The strain tensor $\boldsymbol{St}(s,\vartheta,t)$ is therefore obtained by time integration of the strain rate tensor function, that can be recast as an integration of the unitary tensor over φ, from the undeformed configuration to the generic position $\varphi(t)$

$$\mathbf{St}(s,\vartheta,\varphi) = \int_0^t \mathbf{SR}(s,\vartheta,t)\;dt = \int_0^\varphi \mathbf{SR}_0(s,\vartheta,\varphi)\;d\varphi; \tag{13}$$

Fig. 5 shows the 3 terms of the deformation tensor (13) for $\varphi = 0, \varphi = \pi/4, \varphi = \pi/2$ through a chromatic scale on the surface of the valve for providing a perception of the deformation pattern in the model.

The principal deformations, λ_1 and λ_2, are then evaluated as the eigenvalues of the strain tensor $\boldsymbol{St}$ while the third principal deformation in the direction normal to s and ϑ is obtained by incompressibility constrain as $\lambda_3 = 1/(\lambda_1\lambda_2)$. From these, the strain energy function $W(s,\vartheta,\varphi)$ is evaluated at each point and its surface integral gives the global strain energy function $W(\varphi,t)$. Eventually, the function $F(\varphi)$ to be inserted in the evolution equation (9) is the derivative of $W(\varphi,t)$ with respect to φ. The resulting function is shown graphically in Fig. 6.

2.4. Physical interpretation of the mitral valve parameter

The global elastic coefficient, C, has the dimensions of a frequency. In order to investigate its physical meaning, the elastic recall leading to valvular closure was first analyzed in the absence of blood flow starting from the fully open configuration. In this case, the equation that regulates the valve motion is

$$\frac{d\varphi}{dt} = -CF(\varphi)\,; \tag{14}$$

with initial condition $\varphi(0) = \pi/2$.

When $C > 0$ the valve tends to close; the results of Fig. 7 show that the larger is C and the quicker is the elastic closure. The link between the constant C and the characteristic closing time is found by comparing the instants t_φ in which the opening angle of the valve is reduced to a certain amount φ. Fig. 8 shows the results for reaching a closure $\varphi = \pi/4, \pi/6$ and $\pi/10$ respectively, as C varies, and the bi-logarithmic representation demonstrates that the time to reach the prescribed degree of closure has the form $t_\varphi = A_\varphi C^{-1}$ where the coefficient A_φ depends on the chosen closure angle while the exponential behavior does not.

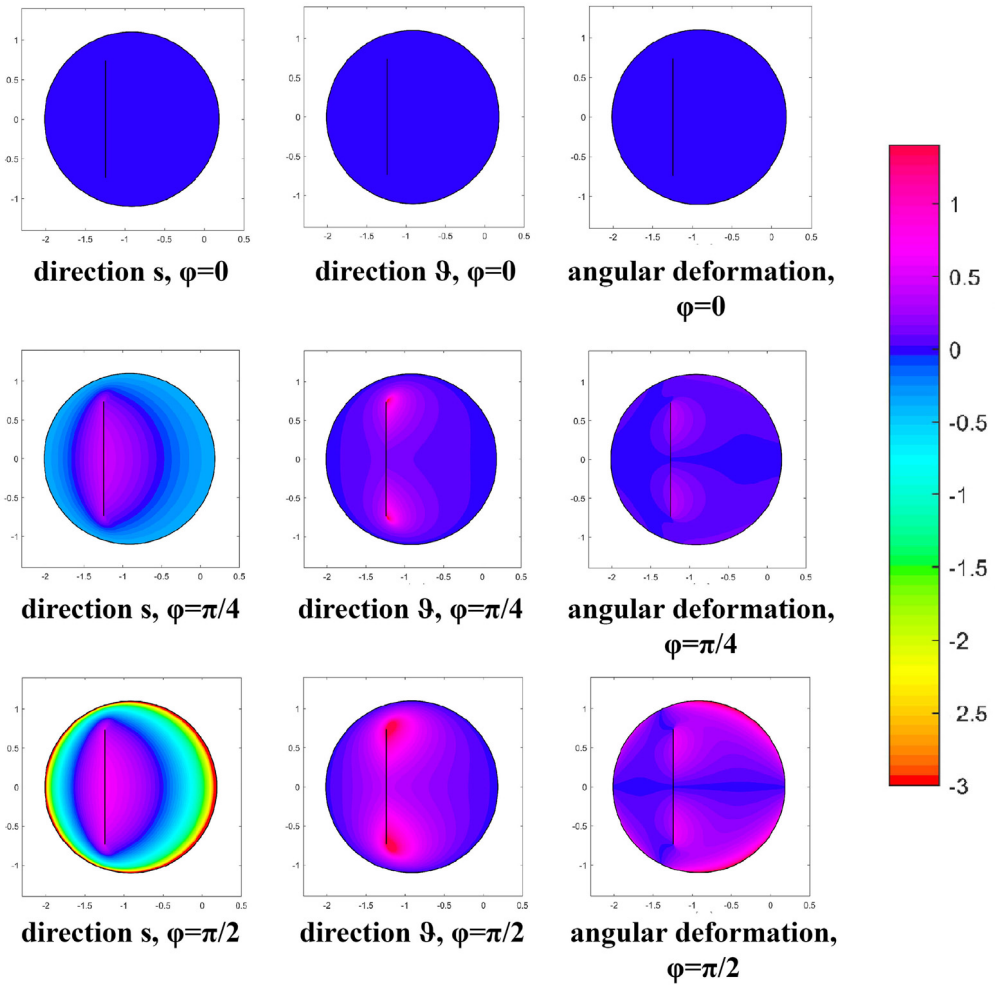

Fig. 5. Valve strain values for $\varphi = 0$, $\varphi = \pi/4$, $\varphi = \pi/2$ represented through a chromatic scale on the surface of the valve. The reference color scale for the strain values is reported on the right. For simplicity, the valve is always represented in its undeformed closed configuration while the colors are used to represent the value of the components of the strain tensor in the different material points of the valve surface. The first column displays the strain along the (radial) direction s, the second column the strain along (circumferential) direction ϑ and the third column displays the shear deformations. The three rows correspond to different degree of opening from undeformed configuration (top row), where all strain values are equal to zero, to opening angle of $\pi/4$ (mid row), to complete opening angle $\pi/2$ (bottom row).

In conclusion, by scaling the time with the parameter C, all the curves in Fig. 7 collapse in a single curve. Therefore, the parameter C is inversely proportional to the valve closure time in absence of blood flow and represents, from a physical point of view, the characteristic response frequency of the valve. This simple parametrization of valvular elasticity was designed to provide an initial understanding of the influence of elastic recall to valvular dynamics.

2.5. Mathematical definition of the fluid problem and numerical method

The fluid–tissue interaction is here simulated using the Immersed Boundary Method. The IBM is a finite difference method which couples a Eulerian description for the blood flow, which is here modeled as a Newtonian incompressible fluid, to a Lagrangian description for the immersed structure. The Eulerian computational domain is a three-dimensional square box described by a Cartesian coordinate system x, y, z. The geometric models of the left ventricle and of the valvular plane containing the mitral and aortic valves are immersed in the computational Cartesian box. The moving surfaces are described by the Lagrangian coordinates of their material points $\boldsymbol{X}(s, \vartheta, t)$, whose velocities therein are $d\boldsymbol{X}/dt$. This velocity is imposed at the corresponding position of the Cartesian grid, thus putting in relation Lagrangian and Eulerian descriptions as extensively described in previously works [15,16].

The initial instant corresponds to the beginning of the diastole phase, here the MV starts from the closed configuration and immediately opens while the aortic valve is closed. The flow starts from rest and the simulation is performed for several heartbeats to ensure the periodicity of the solution and avoid an influence from the initial conditions. For each instant t the position and the velocity of the LV wall are imposed as derived from MRI data. The velocity boundary conditions are imposed on all the solid walls, including the MV leaflets.

The fluid velocity is advanced over time by the Navier–Stokes and continuity equations, written on the Cartesian system of coordinates

$$\begin{aligned} &\frac{\partial \mathbf{v}}{\partial t} + (\mathbf{v}\cdot\nabla)\mathbf{v} = -\nabla p + \nu\nabla^2\mathbf{v} \\ &\nabla\cdot\mathbf{v} = 0 \end{aligned} ; \qquad (15)$$

where t, $\boldsymbol{v}$, p, and ν are the time, velocity, kinematic pressure, and kinematic viscosity ($3,3 \times 10^{-6}$ m^2/s) respectively. The above system of equations is solved in a computational bi-periodic box with a standard fractional step method using a mixed spectral-finite differences scheme, with the LV wall and the MV immersed therein. The Navier–Stokes equation is solved on a 3D staggered

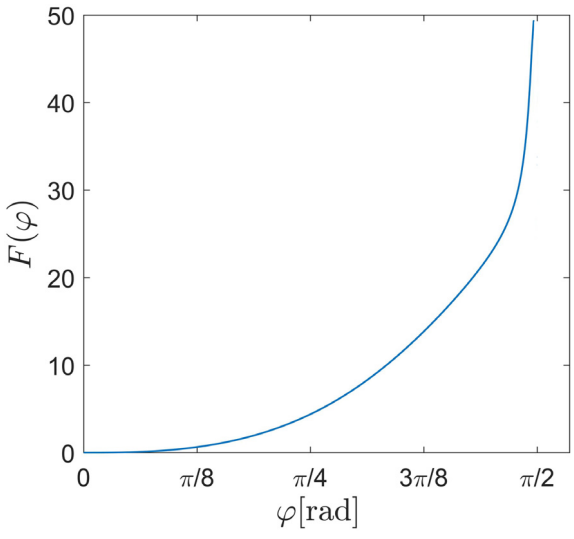

Fig. 6. Graphical representation of the function $F(\varphi)$ for this mitral valve model.

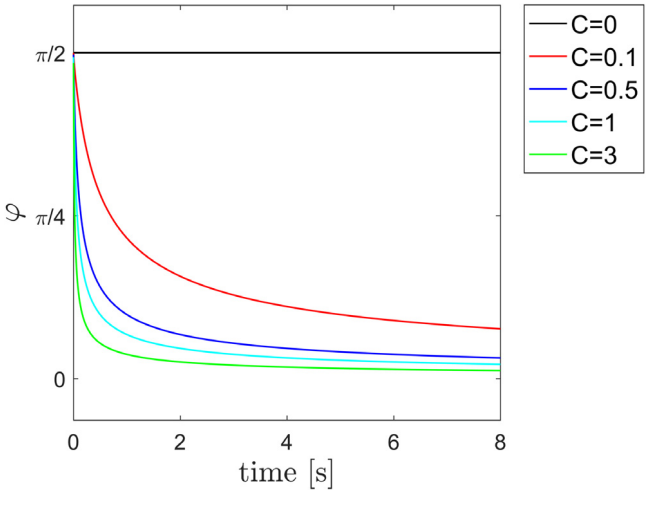

Fig. 7. Opening angle over time as C varies, in the absence of blood flow.

grid with a third order Runge–Kutta method for the temporal advancement. Second order centered finite differences are used for the spatial discretization. The mass conservation is then satisfied solving the Poisson's equation for the instantaneous irrotational correction of the pressure field, which is performed in a x–y Fourier space, allowing fast solutions. At the boundaries along the z direction, free-slip, impermeable boundary conditions are enforced. In parallel to the flow advancement, the motion of the mitral valve is advanced in time using Eq. (9) for the angle $\varphi(t)$. Extensive descriptions of the numerical method and of its validation are given in previous works and they are omitted here [11,17,18]. For reference, in this case simulations are performed on a box of dimension $12 \times 8 \times 8$ cm using a numerical grid $128 \times 128 \times 160$. The time step has been fixed equal to $T/2048$ s, a typical value to satisfy the stability conditions, where T is the heartbeat period assumed equal to 1 s.

3. Results

Complete numerical solutions are performed in correspondence of different values of the MV elastic parameter C with the objective of uncovering the phenomena that are influenced by the mechanical properties of the valve. To this aim, the results relative to the following set of 5 values $C = [0, 0.1, 0.5, 1, 3]$ are analyzed in correspondence of both healthy and dilated LVs.

The most representative parameter of the FTI is the time profile of the opening angle $\varphi(t)$. This is reported in Fig. 9 for the reference case of no elasticity ($C = 0$) with the time profile of LV volume in both the normal and dilated LVs. The valve presents a very rapid opening at the onset of diastole and rapid closure at the onset of systole, with a more irregular pattern in the case of pathological ventricle (which is partly related to the irregularities observed in the motion of the ventricle itself and partly to the weakness of the transmitral flow). The results in Fig. 10 are extended for different values of MV elasticity. They show that the amplitude of opening decreases with increasing value of elastic parameter C, because the valve becomes stiffer and has a larger recall to the undeformed closed position. This behavior is analogous for both normal and dilated ventricle. A remarkable difference between the two cases can be noticed during the diastasis phase when the valve is able to reach a complete closure only in the dilated case (about $t = 0.5$) as $C \geq 0.1$, because the limited transmitral flow is insufficient for keeping the valve open. The opening of the valve during the atrial systole phase is also smaller because the variation in volume determined by the atrial contraction is less intense than in the case of the healthy ventricle. In both cases the valve presents a lower motility for increasing elasticity C.

The decrease of the maximum opening angle φ_{max} for increasing stiffness C is shown in Fig. 11(a). It shows that the maximum

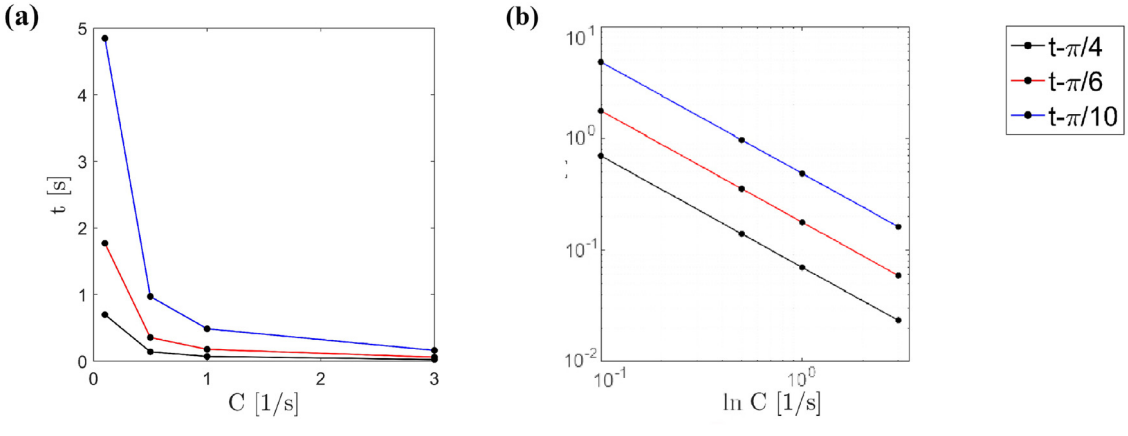

Fig. 8. Time required to reach, in absence of flow, a value of the opening angle equal to $\pi/4$, $\pi/6$ and $\pi/10$ as a function of the elastic parameter C. Linear scales (a) and (b) bi-logarithmic representation.

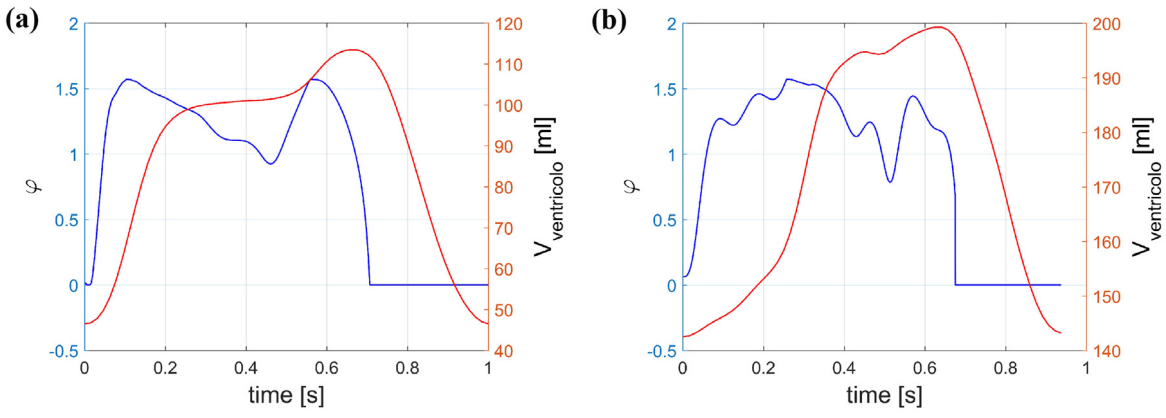

Fig. 9. Time profile of the mitral valve opening angle (left scale) and of the LV volume (right scale) in the reference case of no elasticity $C = 0$ for healthy (a) and dilated ventricles (b).

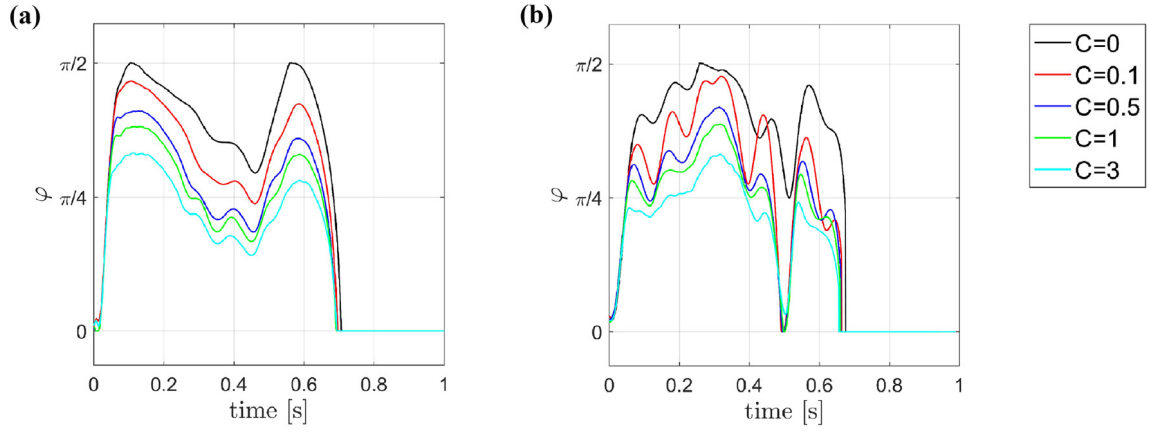

Fig. 10. Time profile of the mitral valve opening angle with varying the parameter C in the case of healthy (a) and dilated ventricles (b).

opening is comparable between the normal and pathological conditions, decreasing with C according to a non-linear law. It is possible to explain this phenomenon considering that the effect of $R(\varphi)$, being proportional to the deformation, is greater in the phase of maximum opening but smaller in the other phases. This mitigates the overall effect of the increasing of the constant C. Differently from before, the timings of mitral valve opening and closure, reported in Fig. 11(b), differ between the case of normal and dilated ventricle as these are dictated by the LV volume rate while they are almost independent from C. These results suggest that the maximum degree of MV opening depends essentially on the mechanical characteristics of the valve and not much on the motion of the ventricle; vice versa, the open/close timings are weakly affected by C as they are driven by the transmitral flow.

The displacement rate, $d\varphi/dt$, of the MV, shown in Fig. 12, shows that the presence of C can either dampen or amplify the fluctuations in the different phases of the cycle, depending on the balance between flow-induced force and the energy stored in the elastic potential when opening is large. The corresponding maximum rate of opening, $d\varphi/dt_{\max}$, and of closure, $d\varphi/dt_{\min}$, are shown in Fig. 13. As expected $\mathrm{d}\varphi/\mathrm{dt}_{\max}$ during the opening phase decreases with increasing C because of the additional resistance given by the valve. The value $\mathrm{d}\varphi/\mathrm{dt}_{\min}$ during closure also decreases in absolute value with increasing C. In this case the opposite would be expected since the closing phase is accelerated by $R(\varphi)$, however, since to a greater value of C corresponds a smaller opening angle $\varphi_{\max}$, the elastic restoring forcing is weaker and this effect is more relevant than the higher elastic recall.

Overall, these results suggest that a characterization of valvular stiffness could be obtained by regular imaging technologies, like echocardiography, by simply reading the maximum degree of opening (or analogous measures of MV opening amplitude) without significant influence or confounding factors associated to differences in LV flow rate. In particular, in the perspective of clinical applications, measurements of MV opening amplitude could reveal variations in stiffness within the same subject over time, thus allow monitoring the progression of a valvular disease.

The valvular elasticity is expected also to have a dynamic influence on the transvalvular pressure gradients between the left heart chambers. The pressure gradient can be viewed as the force required for driving the blood flow and to overcome any resistance encountered by that. The graphs in Fig. 14 show the pressure difference during the diastolic filling phases at varying C values, both for the healthy ventricle (a) and for the dilated one (b). Pressure difference is evaluated between two points across the valve orifice, one on the atrial side and one on the ventricular side at the end of the valve, such that a negative gradient corresponds to a lower ventricular pressure with respect to the atrium. In both cases and for each value of C the gradient is higher during early diastole, when the inlet flow is larger, then it decreases until the left atrium contraction which causes a second peak. This behavior is more evident in the healthy ventricle while the dilated case shows a more irregular pattern due to the fusion between the two diastolic waves. It can be seen how an increase in the value of C corresponds to an increase in the pressure gradient, because the valve is stiffer and makes a higher resistance to flowing; moreover, the maximum opening angle decreases, leading to a narrower mitral orifice that opposes a further higher resistance to the flowing blood. These lead to an increase in the inlet fluid velocity and in the atrium–ventricle

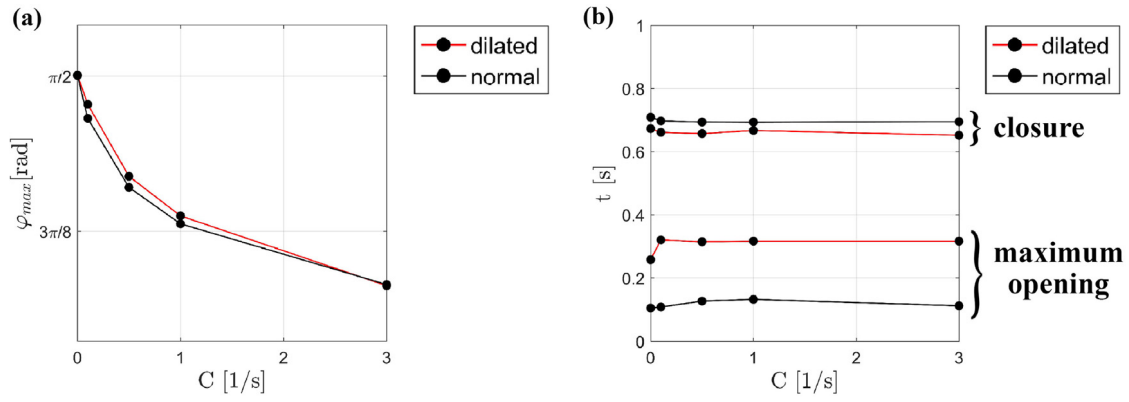

Fig. 11. Maximum opening angle as a function of the parameter C in the case of a healthy ventricle (black) or a dilated ventricle (red) (a). Instants of the complete opening and of complete closure of the valve as function of the parameter C in the case of a healthy ventricle (black) or a dilated ventricle (red) (b).

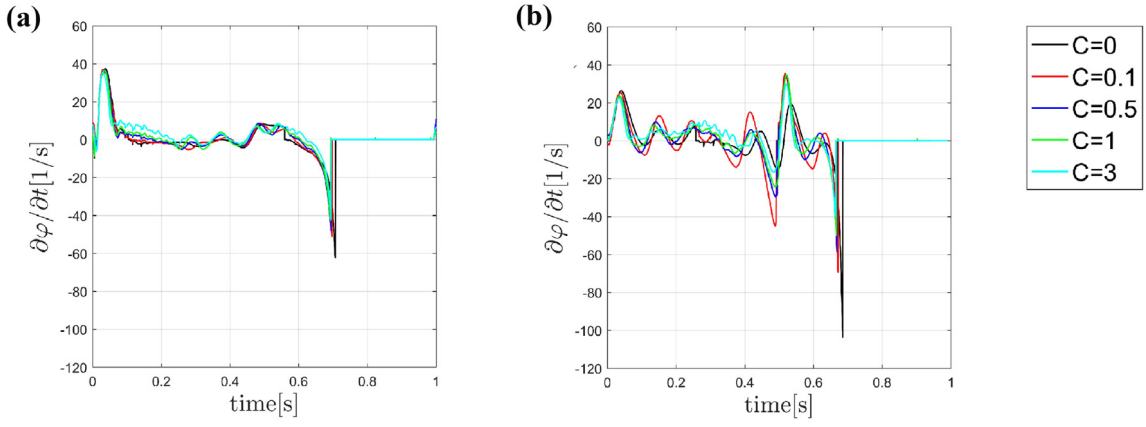

Fig. 12. Valve speed over time as a function of the parameter *C* in the case of the healthy ventricle (a) and in the case of the dilated ventricle (b).

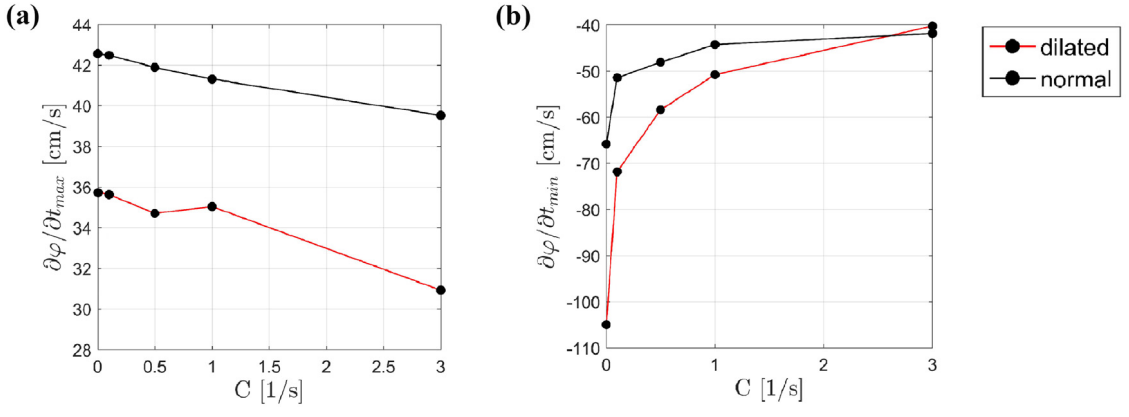

Fig. 13. Maximum opening speed as a function of the parameter *C* in the case of a healthy ventricle (black) or a dilated ventricle (red) (a). Maximum closing speed as a function of the parameter *C* in the case of a healthy ventricle (black) or a dilated ventricle (red) (b).

acceleration that in turn cause an increase in the downstream kinetic energy. This increase in the ventricular blood kinetic energy can then lead to a greater degree of turbulence.

4. Conclusion

This study presents a numerical model of LV fluid dynamics, where the chamber's motion is derived from magnetic resonance images and a simplified fluid–structure interaction model is employed for the MV, with the only aim to understand the influence of leaflets elasticity. An integral approach for MV dynamics is employed to reduce the problem of limited knowledge for individual-specific mechanical properties of the MV tissues and an original formulation of elasticity is introduced. Although a complete solid model with flow–tissue interaction would represent a more rigorous approach to valvular motion, such a rigorous approach requires the specification of material parameters that are not known and not measurable, and introduces the uncertainty about the physical representativeness of those parameters. Having this in mind, the proposed simplified approach, with a valve that is functionally characterized by a single parameter representative of its overall

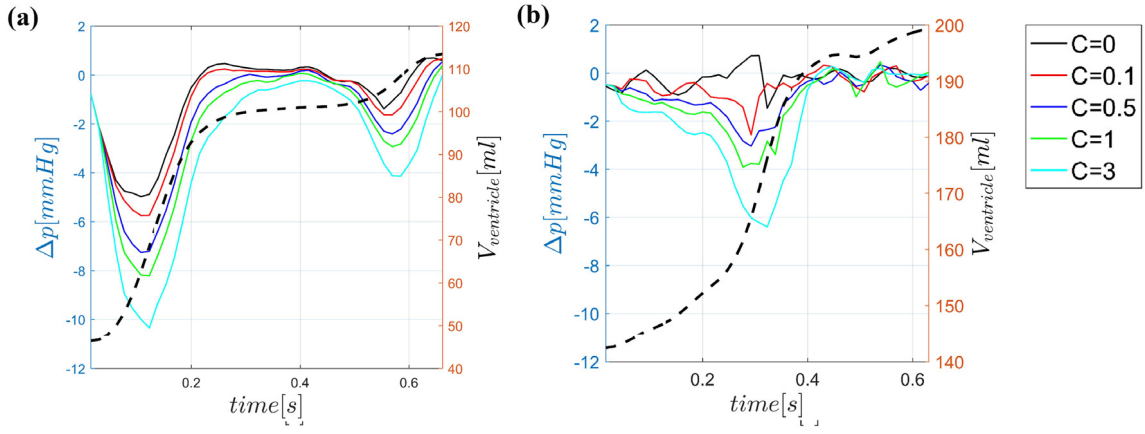

Fig. 14. Pressure gradients across the MV as a function of the parameter C in the case of a healthy ventricle (a) or a dilated one (b), measured during the diastolic phase. The segmented line represents the ventricle volume over time.

mechanical behavior, is used to provide general indications about how an increase of elasticity alters the dynamics of the valvular leaflets, giving a response to elastic recall not qualitatively influenced by the model used.

Results show how the increase of the valvular stiffness has a main influence in terms of reducing valve opening and its maximum velocity, while it does not affect – for a given LV volume rate – the timings of opening and closure that are essentially driven by the transmitral blood flow. The increase of valvular stiffness also influences the transmitral pressure gradients causing significant increases during the diastolic filling phase. This increased gradient is accompanied by a rise in the inlet flow velocity which may give rise to higher degrees of turbulence in the LV.

This is a preliminary study that presents several limitations. The analytical description of the MV represents a first approximation of a realistic anatomical geometry. The valve is also described by a single degree of freedom, while at least two independent leaflets should be considered for realistic models. This was a minimal methodological approach; however, the same approach can extended with relative ease to conditions that are more realistic.

The developed valvular model included a number of simplifications, for example it is characterized by a simple geometry identified by a single degree of freedom. This representation is obviously not entirely realistic, although it allows reproducibility in future studies. On the other hand, models based on few parameters have the chance to allow reliable estimations in patient-specific conditions from the few information effectively available from imaging. These preliminary results suggest a mean for monitoring the variation of valvular stiffness in clinical applications.

References

[1] R. Mittal, J.H. Seo, V. Vedula, Y.J. Choi, H. Liu, H.H. Huang, S. Jain, L. Younes, T. Abraham, R.T. George, Computational modeling of cardiac hemodynamics: Current status and future outlook, J. Comput. Phys. 305 (2016) 1065–1082, http://dx.doi.org/10.1016/j.jcp.2015.11.022.

[2] G. Pedrizzetti, F. Domenichini, Left ventricular fluid mechanics: The long way from theoretical models to clinical applications, Ann. Biomed. Eng. 43 (2015) 26–40, http://dx.doi.org/10.1007/s10439-014-1101-x.

[3] B.E. Griffith, L.H. Charney, X. Luo, D.M. Mcqueen, C.S. Peskin, Simulating the fluid dynamics of natural and prosthetic heart valves using the immersed boundary method, Int. J. Appl. Mech. 1 (2009) 137–177, http://dx.doi.org/10.1142/S1758825109000113.

[4] C.S. Peskin, Flow patterns around heart valves: A numerical method, J. Comput. Phys. 10 (1972) 252–271, http://dx.doi.org/10.1016/0021-9991(72)90065-4.

[5] A. Gilmanov, T.B. Le, F. Sotiropoulos, A numerical approach for simulating fluid structure interaction of flexible thin shells undergoing arbitrarily large deformations in complex domains, J. Comput. Phys. 300 (2015) 814–843, http://dx.doi.org/10.1016/j.jcp.2015.08.008.

[6] V. Meschini, M.D. De Tullio, G. Querzoli, R. Verzicco, Effects of natural and prosthetic mitral valves on the flow structure in healthy and pathological left ventricles, J. Fluid Mech. 834 (2018) 271–307, http://dx.doi.org/10.1017/jfm.2017.725.

[7] K. Kunzelman, D. Einstein, R. Cochran, Fluid–structure interaction models of the mitral valve: function in normal and pathological states, Philos. Trans. R. Soc. B 362 (2007) 1393–1406, http://dx.doi.org/10.1098/rstb.2007.2123.

[8] K.D. Lau, V. Diaz, P. Scambler, G. Burriesci, Mitral valve dynamics in structural and fluid–structure interaction models, Med. Eng. Phys. 32 (2010) 1057–1064, http://dx.doi.org/10.1016/j.medengphy.2010.07.008.

[9] H. Gao, L. Feng, N. Qi, C. Berry, B.E. Griffith, X. Luo, A coupled mitral valve—left ventricle model with fluid–structure interaction, Med. Eng. Phys. 47 (2017) 128–136, http://dx.doi.org/10.1016/j.medengphy.2017.06.042.

[10] H. Gao, N. Qi, L. Feng, X. Ma, M. Danton, C. Berry, X. Luo, Modelling mitral valvular dynamics–current trend and future directions, Int. J. Numer. Methods Biomed. Eng. 33 (2017) 1–15, http://dx.doi.org/10.1002/cnm.2858.

[11] F. Domenichini, G. Pedrizzetti, Asymptotic model of fluid–tissue interaction for mitral valve dynamics, Cardiovasc. Eng. Technol. 6 (2015) http://dx.doi.org/10.1007/s13239-014-0201-y.

[12] J.H. Seo, V. Vedula, T. Abraham, A.C. Lardo, F. Dawoud, H. Luo, R. Mittal, Effect of the mitral valve on diastolic flow patterns Effect of the mitral valve on diastolic flow patterns, Phys. Fluids 26 (2014) 121901, http://dx.doi.org/10.1063/1.4904094.

[13] G. Pedrizzetti, P.M. Arvidsson, J. Töger, R. Borgquist, F. Domenichini, H. Arheden, E. Heiberg, On estimating intraventricular hemodynamic forces from endocardial dynamics: A comparative study with 4D flow MRI, J. Biomech. 60 (2017) 203–210, http://dx.doi.org/10.1016/j.jbiomech.2017.06.046.

[14] G. Pedrizzetti, E. Kraigher-Krainer, A. De Luca, G. Caracciolo, J.O.J.O. Mangual, A. Shah, L. Toncelli, F. Domenichini, G. Tonti, G. Galanti, P.P.P. Sengupta, J. Narula, S. Solomon, Functional strain-line pattern in the human left ventricle, Phys. Rev. Lett. 109 (2012) 048103, http://dx.doi.org/10.1103/PhysRevLett.109.048103.

[15] R. Mittal, G. Iaccarino, Immersed boundary methods, Annu. Rev. Fluid Mech. 37 (2005) 239–261, http://dx.doi.org/10.1146/annurev.fluid.37.061903.175743.

[16] F. Domenichini, On the consistency of the direct forcing method in the fractional step solution of the Navier–Stokes equations, J. Comput. Phys. 227 (2008) 6372–6384, http://dx.doi.org/10.1016/j.jcp.2008.03.009.

[17] J.O. Mangual, F. Domenichini, G. Pedrizzetti, Three dimensional numerical assessment of the right ventricular flow using 4D echocardiography boundary data, Eur. J. Mech. B/Fluids 35 (2012) 25–30, http://dx.doi.org/10.1016/j.euromechflu.2012.01.022.

[18] J.O. Mangual, E. Kraigher-Krainer, A. De Luca, L. Toncelli, A. Shah, S. Solomon, G. Galanti, F. Domenichini, G. Pedrizzetti, Comparative numerical study on left ventricular fluid dynamics after dilated cardiomyopathy, J. Biomech. 46 (2013) 1611–1617, http://dx.doi.org/10.1016/j.jbiomech.2013.04.012.